

Structural studies on the full-length self-assembled histone-like nucleoid structuring protein (H-NS) using solid-state NMR spectroscopy

Marie Renault¹, Jesús García³, Tiago N. Cordeiro³, Marc Baldus^{1*} and Miquel Pons^{2,3*},

¹Bijvoet Center for Biomolecular Research, Utrecht University, Padualaan 8, 3584 CH Utrecht, The Netherlands; ²Laboratory of Biomolecular NMR, Department of Organic Chemistry, University of Barcelona, Baldiri Reixac, 10, 08028-Barcelona, Spain; ³Institute for Research in Biomedicine, Parc Científic de Barcelona, Barcelona, Spain.

* To whom correspondence should be addressed: m.baldus@uu.nl or mpons@ub.edu

Present address: MR, Institute of Pharmacology and Structural Biology, UMR 5089, CNRS, 205 route de Narbonne, BP 64182, 31077 Toulouse, France; TNC, Centre de Biochimie Structurale, CNRS, 29, rue Navacelles 34090 Montpellier, France.

Title running head: Solid-state NMR on H-NS proteins.

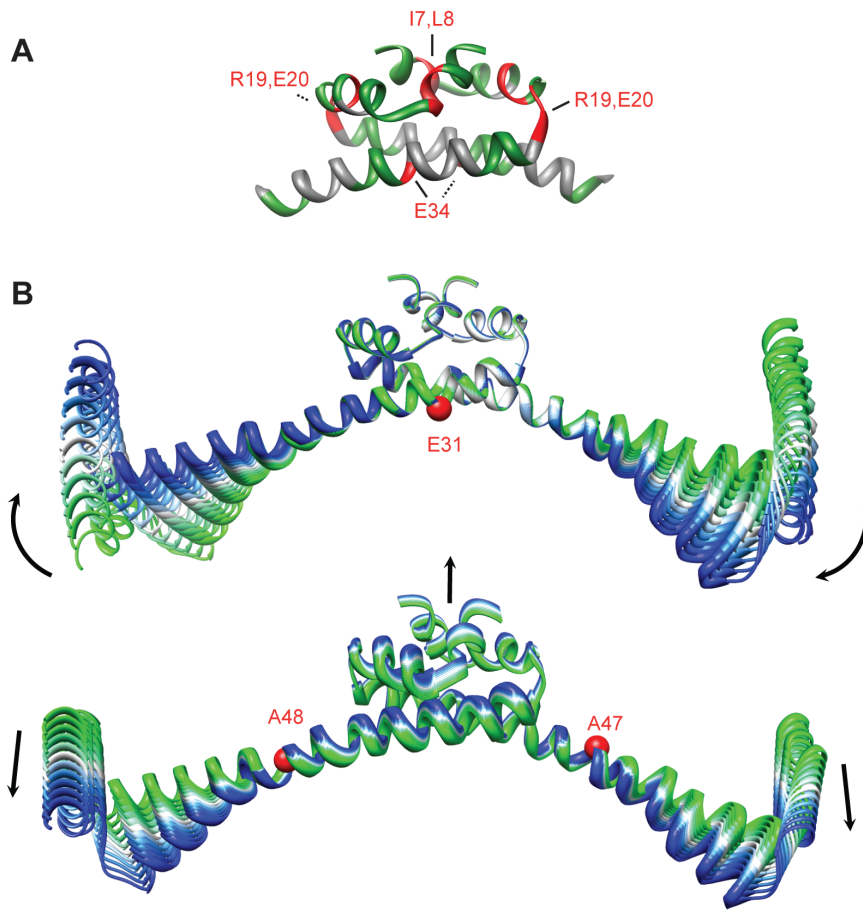


Figure 7

Abstract

Members of the histone-like structuring protein (H-NS) family play roles both as architectural proteins and as modulators of gene expression in Gram-negative bacteria. The H-NS protein participates in modulatory processes that respond to environmental changes in osmolarity, pH or temperature. H-NS oligomerization is essential for its activity. Structural models from different truncated forms are available. However, high-resolution structural details of full-length protein H-NS and its DNA bound state have largely remained elusive. We report on progress to characterize the biologically active H-NS oligomers using solid-state NMR spectroscopy (ssNMR). We have compared uniformly (^{13}C , ^{15}N)-labeled ssNMR preparations of the isolated N-terminal region (H-NS 1-47) and full-length H-NS (H-NS 1-137). In both cases, we obtained ssNMR spectra of good quality and characteristic of well-folded proteins. Analysis of two- and three-dimensional (^{13}C , ^{13}C) and (^{15}N , ^{13}C) correlation experiments conducted at high field led to assignments of residues located in different topological regions of the free full-length H-NS protein. These findings confirm that the structure of the (N-terminal) dimerization domain is conserved in the oligomeric full-length protein. Small changes in the dimerization interface suggested by localized chemical shift variations between solution and solid-state spectra may be relevant for DNA recognition.

Database. Structural data are available in the BioMagResBank database (BMRB; <http://www.bmrwisc.edu>) under the accession number 18814.

Keywords: chromatin, H-NS, sequential assignment, solid-state NMR.

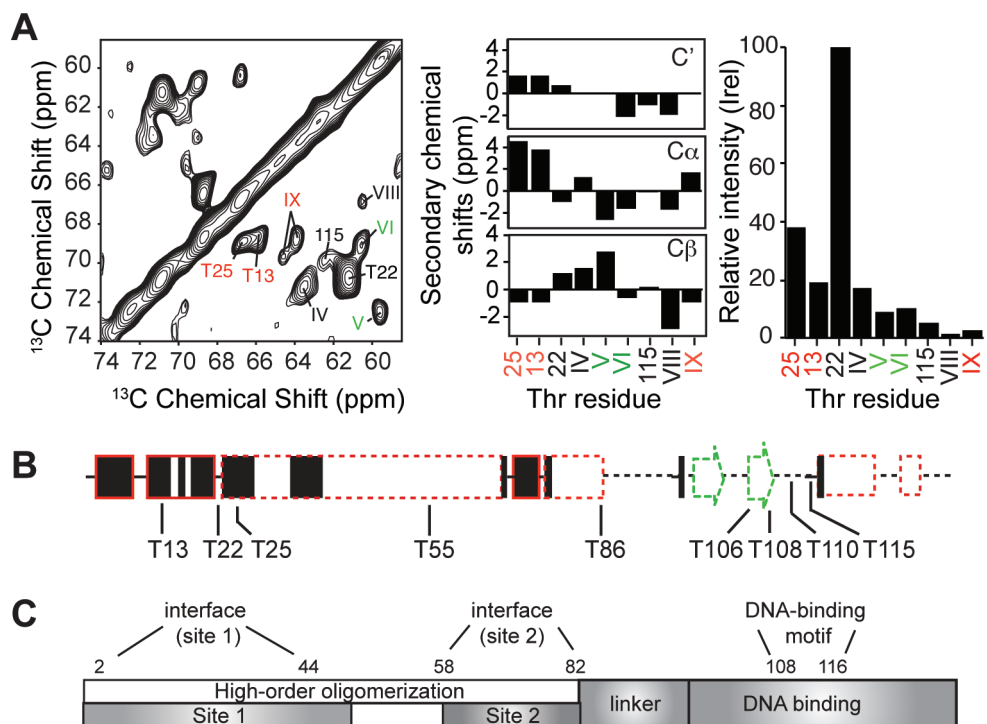


Figure 6

Introduction

The chromosomal DNA of bacteria is folded into a compact nucleoid body that is constantly remodeled in response to environmental signals. The folding is attributed in part to interactions with abundant nucleoid-associated proteins (NAPs), such as DNA bridging proteins. As with eukaryotic DNA, gene compaction via protein condensation and changes in accessibility to promoter regions provide general mechanisms to control gene expression within the bacterial nucleoid. The histone-like nucleoid structuring protein (H-NS) is a highly abundant and ubiquitous DNA-binding protein of 15.4 kDa that plays essential roles in the organization [1] and the compaction of bacterial chromatin. H-NS acts as a global regulator of gene expression, including laterally acquired genes [2-4] and those involved in bacterial adaptation to environmental changes [5, 6] and plays important roles in bacterial physiology and virulence. H-NS consists of an N-terminal oligomerization domain (residues 1-82) and a C-terminal DNA binding domain (residues 95-137), functionally independent and linked by a flexible connection allowing for fast local molecular motions. Although the molecular basis of H-NS activity is not fully understood, the oligomerization of the protein is crucial for its biological activity. Local DNA recognition by the C-terminal domain involves indirect readout of DNA minor groove distortions [7]. The weak affinity of individual domains is compensated by cooperative binding of H-NS oligomers. Simultaneous reading of properly positioned neighbour DNA regions requires complementary geometries of DNA and H-NS oligomers and the modulation of the oligomerization process may provide a mechanism to increase its affinity. Oligomerization can induce higher order structures by promoting the formation of loops or stiffening of DNA [8-10]. Similar mechanisms have been observed for structurally distinct proteins sharing similar functions in mycobacteria and pseudomonas [11, 12]. Considerable efforts have been made during the last decades to unravel the structure and

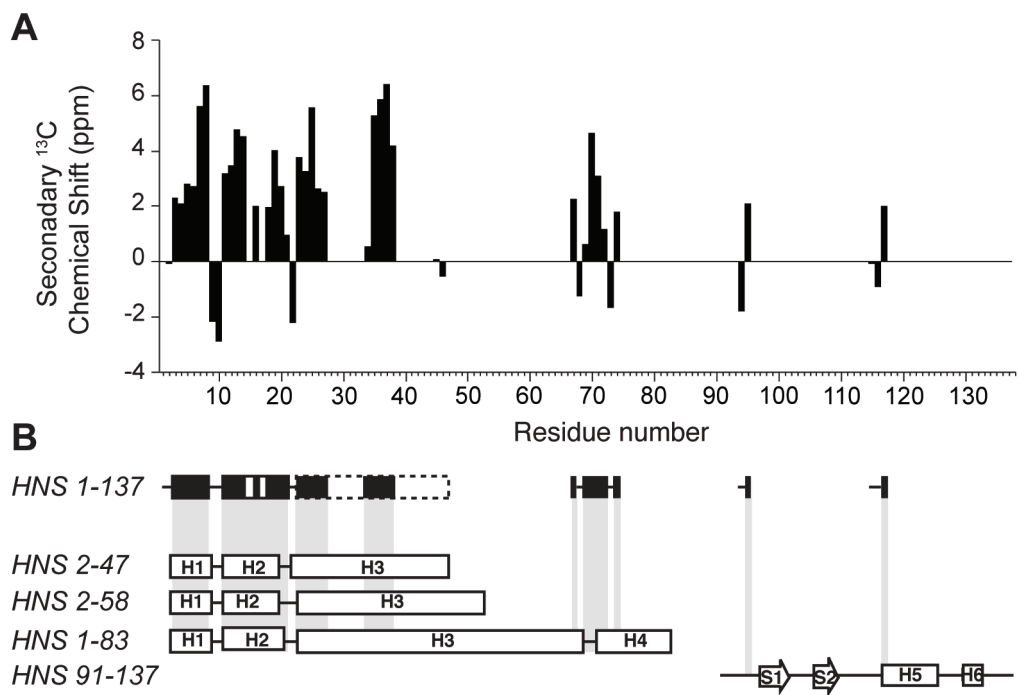


Figure 5

roles of H-NS proteins at the atomic level. Structural models for H-NS oligomerization and DNA binding have been determined for different organisms using solution-state NMR spectroscopy and X-ray crystallography on truncated versions of H-NS (*Salmonella typhimurium*, residues 2-58 [13], 2-65 [14], 1-83 [15] and 91-137[16]; *Escherichia coli*, residues 2-47 [17] and 91-137 [18]; and *Vibrio cholerae*, residues 2-51 [19]). The structure of the highly homologous C-terminal domain of Ler in complex with a 15mer DNA duplex has been recently solved [7]. However, the structural characterization of the full-length H-NS proteins still remains elusive due to the large size of self-assembled H-NS complexes and their intrinsic flexibility.

Solid-state NMR (ssNMR) under Magic Angle Spinning (MAS) [20] conditions has made considerable progress in the structural study of proteins in the context of amyloid formation or when associated with membranes. So far, only few studies have been reported on protein systems known to interact with DNA or RNA. Quadrupolar ssNMR was used on a minimal DNA Binding Domain of Human Nucleotide Excision Repair Protein XPA [21] and ssNMR probed protein structure and dynamics Pf1 bacteriophage [22]. In the following we show that high-resolution ssNMR spectra can be obtained from full length H-NS and partially assigned, providing atomic resolution probes located in different important regions of the protein sequence. These results highlight the hinge role of the N-terminal dimerization domain and suggest that interactions in this region may modify the geometry of the resulting oligomers. The results reported herein open the way for structural studies of different proteins of the H-NS family and their interaction with other proteins or DNA.

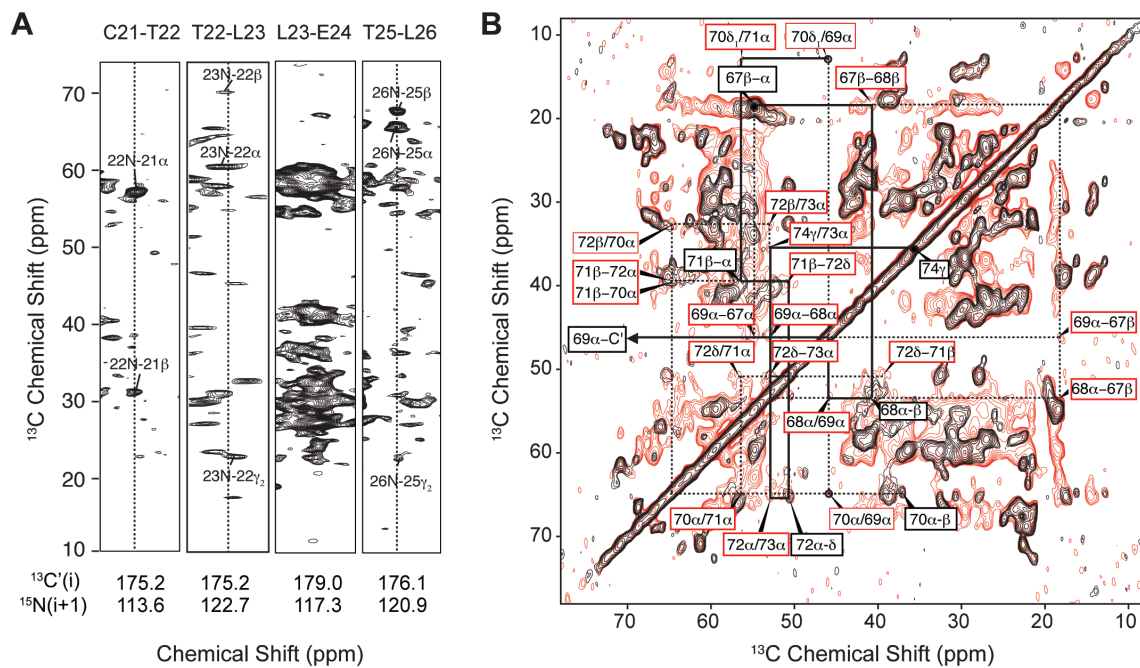


Figure 4

Results

2D and 3D ssNMR correlation experiments on self-assembled H-NS oligomers

Fig. 1 displays two-dimensional proton-driven ^{13}C - ^{13}C spin-diffusion (top) and NCACX (bottom) spectra obtained on functionally active oligomers of the full-length (U- ^{13}C , ^{15}N)-labeled H-NS protein from *E. coli*. In addition, a 2D NCOCX spectrum is given in supporting information (Supplementary Information, Fig. S1). The spectral resolution is given by ^{13}C and ^{15}N linewidths of 0.9 and 1.6 ppm respectively, and compares favorably to ssNMR data obtained on microcrystalline globular proteins [23, 24]. Whilst the spectral resolution is high, significant spectral overlap due to the predominantly α -helical nature of the protein and the high occurrence of particular amino-acid types (especially Ser, Ala, Arg, Glu, Leu, Lys and Val) complicate the assignment process. In this context, we complemented our data with a series of 2D ssNMR experiments on (U- ^{13}C , ^{15}N)-labeled H-NS (1-47), a truncated form of the H-NS protein corresponding to the minimal dimerization domain of H-NS [17]. This sample is likely to facilitate the assignment procedure since up to 83 % of the most abundant and spectrally overlapped amino-acid types (Ser, Ala, Arg, Glu, Leu, Lys and Val) from the full length H-NS protein are removed. Fig. 2A displays an overlay between the two-dimensional proton-driven ^{13}C - ^{13}C spin-diffusion correlation spectra of (U- ^{13}C , ^{15}N)-labeled full-length H-NS and its truncated variant H-NS 1-47 obtained under identical measurement conditions. Interestingly, both preparations exhibit similar spectral resolution for isolated resonances indicating a comparable structural order between the self-assembled full-length protein and the isolated N-terminal dimerization domain. In addition, the intraresidue CC correlation pattern of H-NS 1-47, which dominates the proton-driven ^{13}C - ^{13}C spin-diffusion spectrum acquired with short mixing time, is largely conserved within the full-length H-NS spectrum (Supplementary Information, Fig. S2). For the full-length H-NS preparation, we identified

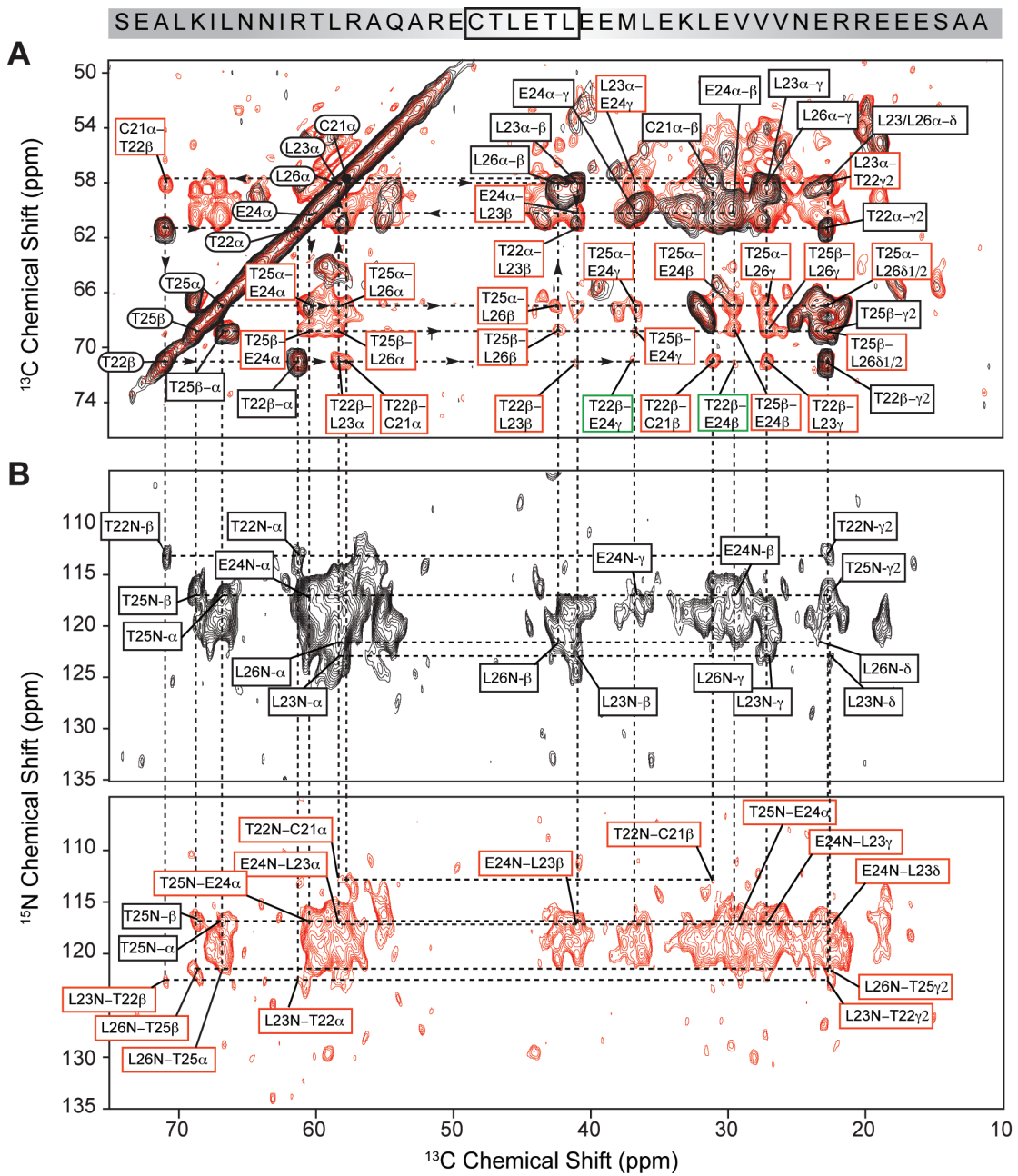


Figure 3

^{13}C spin-systems of all Thr (Fig. 2A, I to IX) and Pro (Fig. 2A, X to XII) residues, which are well distributed within the protein sequence (Fig. 2B). According the standard amino acid-specific peak positions and chemical-shift dispersion of individual $\text{C}\alpha$ and $\text{C}\beta$ resonances, H-NS exhibits rigid protein segments within α -helical and β -sheet secondary structure elements as well as in unstructured protein regions, in accordance with the expected topological profile (Fig. 2B). Interestingly, both cross-peak position and relative intensity of Thr I, II and III from the N-terminal domain are well preserved in both preparations. Only subtle chemical shift variations are observed for backbone resonances of Ser residues that are located at the N- and C-terminus ends of the H-NS 1-47 construct. Altogether, these observations strongly suggest that H-NS is well folded in both preparations and that the global fold of the N-terminal domain of the full-length H-NS is largely conserved within the truncated form.

Because of the favorable spectroscopic dispersion for certain residue types (such as Thr and Pro) and the large spectral similarities between the full-length and the truncated H-NS protein preparations, we could subsequently perform a residue-specific analysis of H-NS by using a strategy consisting in 3 steps. First we determined sequential resonance assignments for the H-NS 1-47 sample in spectroscopically favorable regions. Second, comparison to the same spectral regions in datasets obtained for full-length H-NS served to obtain tentative assignments for the same residues in the full construct. Finally, correlations were cross-validated using additional 2D and 3D datasets of ($\text{U-}^{13}\text{C},^{15}\text{N}$)-labeled full-length H-NS and extended to residues located in other topological regions of the protein.

Fig. 3 shows an example of the sequential assignment process performed on the ($\text{U-}^{13}\text{C},^{15}\text{N}$)-labeled H-NS 1-47 using a combination of two-dimensional ^{13}C - ^{13}C and ^{15}N - ^{13}C ssNMR correlation spectra. The 2D PDSF experiment conducted under weak-coupling conditions [25] using long mixing time revealed a variety of sequential connectivities, particularly apparent in the spectral region between 45 and 70 ppm where only intra-residue

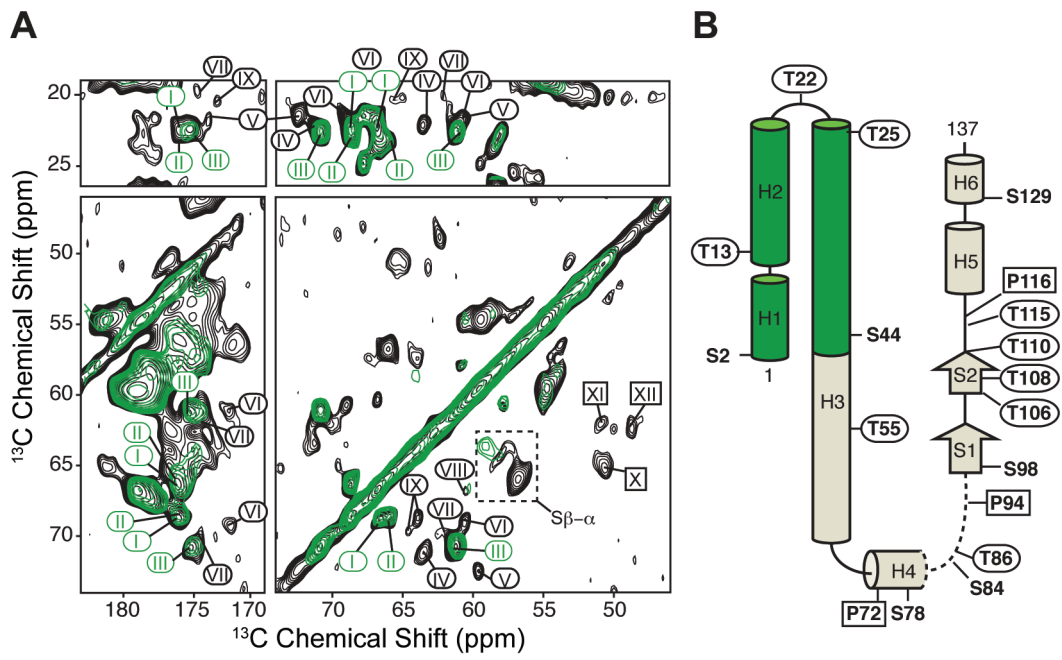


Figure 2

correlations for Ser, Thr and Pro residues are possible (Fig. 3A). In addition, a 2D NCACX (Fig. 3B) and NCOCX (Fig. 3C) spectra were recorded to cross-validate sequential information using ^{15}N - ^{13}C type correlations and obtain assignments of higher reliability. In such experiments, the discrimination between intra- and inter-residue cross-peaks is realized by use of SPECIFIC CP [26] transfers, where $^{15}\text{N}_i$ - $^{13}\text{C}\alpha_i$ or $^{15}\text{N}_i$ - $^{13}\text{C}'_{i-1}$ connectivities are specifically established. Magnetization transfer along the carbon sidechain were obtained by adding a PARIS [27] or MIRROR [28] irradiation schemes as mixing after the SPECIFIC CP, which result in $^{15}\text{N}_i$ - $^{13}\text{C}\alpha_i$ - $^{13}\text{C}\alpha_{i+1}$ (NCACX) or $^{15}\text{N}_i$ - $^{13}\text{C}'_{i-1}$ - $^{13}\text{C}\alpha_{i+1}$ (NCOCX) type correlations, respectively. Using this strategy, sequential assignments could be obtained for 33 (70 %) of the 47 residues of H-NS N-terminus domain. Missing assignments correspond to Glu/Arg clusters of up to 6 residues, for which ^{13}C and ^{15}N resonance frequencies exhibited spectral overlap.

Data from 2D ^{13}C - ^{13}C and ^{15}N - ^{13}C correlation experiments obtained on truncated H-NS were compared and combined with those obtained on full-length H-NS sample to derive sequential resonance assignments for H-NS dimerization domain (1-47). In addition, a 3D NCOCX experiment was performed on the full-length (U - ^{13}C , ^{15}N) H-NS sample to resolve sequential ^{15}N - ^{13}C -correlation information in an additional dimension and to complete a formal backbone walk. Fig. 4A displays selected strips extracted from the 3D NCOCX spectrum, showing sequential $^{15}\text{N}_i$ - $^{13}\text{C}_{i-1}$ correlations for residues in the N-terminus domain of full-length H-NS. Approximately, 25% of backbone resonance arising from the N-terminal domain could be confirmed from this experiment. Further attempts to extend backbone sequential walks were hampered by a significant overlap of ^{15}N resonances in the region 116-119 ppm (Fig. 4A). Nevertheless, the comparison between 2D proton-driven ^{13}C - ^{13}C spin-diffusion correlation spectra of truncated and full-length (U - ^{13}C , ^{15}N)-labeled H-NS preparations allowed for the identification of residues from other topological regions of the

protein. In particular, the Pro residues are absent from the N-terminal domain and exhibit well-dispersed and isolated C α -C δ correlations that constitute valuable starting points for sequential walk within the linker and the C-terminus domain. Using sequential CC connectivities arising in the 2D proton-driven ^{13}C - ^{13}C spin-diffusion correlation spectrum of H-NS at long mixing time, we could identify signals of Pro72, Pro94, Pro116 and neighboring residues. An example of sequential assignment from the region around Pro72 is given in Fig. 4B. Altogether, ssNMR assignments could be obtained for 46 (33%) of all 137 residues of full-length H-NS, encompassing the N-terminus dimerization domain, the second dimerization site contributing to oligomer formation, the linker region connecting the oligomerization and DNA binding domains, and the C-terminus DNA-binding region. Assigned residues are indicated in Fig. 1 and listed in Supplementary Information, Table S1.

Structural analysis

Using residue-specific ssNMR assignments, we determined secondary chemical shifts that reflect the conformation-dependent chemical shift of C α and C β resonances of H-NS and related the experimentally observed carbon chemical shifts under MAS conditions to standard isotropic random coil values (BioMagResBank, <http://www.bmrb.wisc.edu>), as described previously [29]. Using these experimental values, we could identify characteristic helical and non-helical stretches within self-assembled full-length H-NS protein. Fig. 5A shows ssNMR secondary chemical shifts as bars, where positive values correspond to α -helical secondary structure. We subsequently compared their distribution with those identified in high-resolution three-dimensional structures of truncated H-NS variants (Fig. 5B). Helical regions as revealed from our data are shown with horizontal bars (filled rectangles) at the top, while secondary structures elements found in the solution NMR structures of *E. coli* H-NS 2-47 [17], 2-58 [13], 91-137 [18] and in the crystal structure of mutated *S. typhimurium* H-NS 1-

83 [15] are indicated as references at the bottom (open rectangles). In the dimerization domain of H-NS (residue 1 to 47), we found α -helical structures in the regions between residues Glu3-Leu8, Ile11-Cys21, Leu23-Glu27 and Glu34-Asn38. Although not complete, secondary chemical shifts computed from our ssNMR analysis are in very good agreement to helical segments found in high-resolution structures of truncated H-NS proteins. The helical boundary regions between helices 1 and 2 are well defined by our data and indicate that Asn9 and Asn10 form a short and unstructured segment linking the two helices. Thr22 does not present chemical shifts typical of a helical structure and marks the boundary between helices 2 and 3. Regarding helix 3, if continuity is assumed between E28 and L33 residues, ssNMR and solution NMR data are in good agreement since both are consistent with a α -helix covering at least residue 23 to 46. In the linker region, ssNMR secondary chemical shifts indicate the presence of a turn (Asp67 and Gly68) followed by an additional helical segment from residues Ile70 to Glu74 in the full-length H-NS. Whilst we cannot infer the continuity of this α -helical segment due to missing assignments, this conformation closely mirrors the second site of dimerization seen in the crystal structure of the truncated H-NS 1-83 protein that is formed by a helix-turn-helix motif between residues 57 and 83 [15]. In the DNA binding domain, we found random coil chemical shifts for residues Pro94, Thr115 and Pro116 and a strong α -helical secondary chemical shift for Ala117, in agreement with the solution NMR structure of the isolated H-NS C-terminus domain (residues 91-137) [16, 18, 30]. Even without sequential assignment, additional structural information can be obtained from the amino-acid specific analysis of H-NS ssNMR spectra within well-dispersed spectral regions. In particular, the analysis of the intraresidue ^{13}C - ^{13}C correlation patterns of threonines, which are readily visible in the 2D PDS spectrum of H-NS 1-137 (Figure 6A, left), offers a means to probe secondary structure elements within uncharacterized protein regions, including the short linker region connecting the oligomerization (1-82) and DNA-

binding (95-137) domains which remains structurally elusive. Experimental secondary chemical shifts of all threonine residues are presented as bars in Figure 6A (middle), with corresponding sequential assignment when available. Positive values of $\Delta\delta C'$ and $\Delta\delta C\alpha$ indicate helical secondary structure, whereas negative values are characteristic of β -sheet protein segment. Conversely, negative and positive values of $\Delta\delta C\beta$ indicate α -helical and β -sheet elements, respectively. Among unassigned threonine residues, Thr residue V exhibits negative values $\Delta\delta C\alpha$ and positive values for $\Delta\delta C\beta$ that typify β -sheet protein segments. Thr IV and VIII exhibit $\Delta\delta C\alpha$ and $\Delta\delta C\beta$ values of the same sign, which may correspond to unstructured regions. Different secondary structure predictions based on different nuclei are also found for Thr VI. However in this case, large negative $\Delta\delta C'$ and $\Delta\delta C\alpha$ and a small value of $\Delta\delta C\beta$ would be compatible with a β -sheet environment. Thr IX shows polymorphic character with two populations characterized by α -helix like secondary $^{13}C\alpha$ and $^{13}C\beta$ chemical shifts. (Fig. 6A, left). Overall, these data are consistent with the topological model of H-NS that emerges from available high-resolution structural data (Fig. 6B): 2 Thr in β -sheet conformation (Thr106 and Thr108), 4 Thr in random coil conformation (Thr22, Thr86, Thr110 and Thr115) and 3 Thr in α -helical secondary structure (Thr13, Thr25 and Thr55). Since Thr13 and Thr25 could be assigned independently, Thr IX is therefore tentatively assigned to Thr55 that is located in α -helical region next to the second dimerization site of H-NS and appears in two different environments in the solid-state samples suggesting structural heterogeneity. Thr V and Thr VI could be assigned to Thr106 and Thr108 that are located in the DNA binding domain β -sheets. Finally, Thr IV and Thr VIII that give intense and well-resolved $C\alpha$ - $C\beta$ cross-peaks and display random-coil ^{13}C chemical shifts may correspond to Thr86 located in the so far structurally elusive linker region and Thr110 from the DNA binding domain. Thr110 indeed belongs to a previously identified loop region in the DNA binding domain [16,18]. To complement our analysis data, we measured and compared

the relative intensity of Thr C α /C β cross-peaks (Fig. 6A, right). We observed a sizable and homogeneous attenuation in NMR signal intensity for Thr V, VI, and Thr115, located in the C-terminus regions as compared to Thr13, Thr25 and Thr22 located in the oligomerization N-terminus domain of H-NS. The low intensity of Thr IX (Thr55) arises from signal duplication (Fig. 6C). Residue Thr IV exhibits similar peak intensity to residues located in the first dimerization site e.g. Thr13, Thr25 and Thr VIII has intensity comparable to residues located in the DNA binding domain. We thus speculate that Thr VIII corresponds to residue 110 and Thr IV to residue 86 in the linker region.

To better define the differences between our data and available structural information obtained on truncated H-NS constructs, we next performed a comparative analysis in reference to experimental C α solution NMR chemical shifts. Solution NMR chemical shifts of H-NS 1-47 were measured and assigned independently by using a standard set of double and triple resonance experiments on the (U-¹³C,¹⁵N)-labeled construct. (Supplementary Information, Table S2). Those of the H-NS 2-58 construct were obtained from BioMagResBank (BMRB 5390). The results are shown as a bar plot of C α secondary chemical shifts for the different datasets (Supplementary Information, Fig. S3) and as a color code of C α chemical shift differences mapped onto the structural model of HNS 2-47 (Fig. 7A). Residues colored in red exhibit C α chemical shifts changes greater than 2 ppm when comparing solution NMR shifts. Not surprisingly, the best overall agreement is obtained when exactly the same molecule (H-NS 1-47) is measured in solution and solid state. However, significant chemical shift deviations are observed in all cases for residues Ile7 and Leu8 in helix 1, Arg19 and Glu20 as part of helix 2 and Glu34 located in helix 3. These residues are situated close to the loops connecting the three helical segments in each monomer or at the dimer interface, involving notably helix 3. In the antiparallel topology observed either by solution NMR or by crystallography in most of the constructs, the regions

of maximum chemical shift changes suggest hinge points in the N-terminal dimerization domain. The possible structural implications are discussed below.

Discussion

In this study, we have provided first structural information of functional and self-assembled variants of full-length H-NS proteins from *E. coli*. We reported *de novo* ssNMR assignments for 33 % of the residues of the entire protein and 70% of the N-terminal dimerization domain, which were obtained by using different protein constructs and a complete set of multidimensional ssNMR pulse sequences. Taken together our ssNMR analysis, albeit based on incomplete sequential assignments at this point, suggests that earlier structural evidence obtained on shorter H-NS constructs is also valid in the full-length H-NS. In detail however, our results point to structural heterogeneity in the N-terminal helices 1 and 2 as well as the helical region containing Thr55. Both segments are remarkably close to the dimerization sites observed in the recent X-ray structure of the 1-83 truncated form of H-NS. The first dimerization site corresponds to the dimer observed in the 2-47 truncated form and involves also helices H1 and H2. A second dimerization site is formed by a helix-turn-helix motif between residues 57 and 83 (Fig. 6C). This site is further stabilized by salt bridges between Arg54-Glu74* and Lys57-Asp68* (residues marked with * are from a different molecule). Thr55 identified in our work as polymorphic is located next to the second dimerization site. The duplicate signals would be consistent with the coexistence of different oligomeric arrangements (or free and bound forms) in the same preparation. The structural heterogeneity may explain the difficulties in the assignment of the oligomerization interfaces. On the other hand, H-NS DNA targets are generally recognized by an array of binding domains within H-NS oligomers. Individual H-NS DNA binding domains show relatively weak affinities and

cooperative interaction of several domains is required to ensure efficient binding. The short linker region connecting the oligomerization and DNA binding domains has been recently demonstrated to play an essential role in the capacity of H-NS variants to differentiate between horizontally acquired and core DNA [31]. In particular, the flexibility of this linker region in the presence of DNA was suggested to be a key element in the selectivity of H-NS towards the two DNA classes. The linker region is absent in any of the previous structural models based on truncated forms. Our ssNMR data on residue 86 are compatible with an unstructured but rigid linker region, even in the absence of DNA. Interestingly, the linker region 87-96 contains four positively charged amino acids. Arg 90 and Arg 93 were shown to interact with DNA and mutations in this region dramatically change the properties of the nucleoprotein complexes [31].

The role of the linker region can be understood in the context of indirect readout of DNA. Individual Ler and H-NS domains recognize local distortions of DNA minor groove widths [7] rather than specific local DNA sequences. To differentiate longer DNA segments, indirect readout can be established by constraining the capacity of several DNA binding domains of an H-NS oligomer to interact simultaneously with DNA. According to the recent oligomerization model suggested by the Ladbury group, the first dimerization site plays a key role in determining the relative orientation of the H3 helices and, therefore, of the attachment point of the DNA binding domains. The new data suggest a connection between the orientation of the long H3 helices and structural features affecting the packing of the N-terminal dimerization domain. This connection may be functionally very relevant. It is known that binding of co-regulators of the Hha family to the N-terminal dimerization domain causes a change in the selectivity of H-NS oligomers towards xenogenic DNA in a similar way than changes in the linker region [2, 31]. Indeed, small structural changes in the N-terminal dimer interface, or changes in the linker region, could significantly change the

relative position of adjacent DNA contact points and, therefore, modulate the recognition of long-range DNA shape distortions. Significant chemical shift differences between experimental H-NS solid-state and solution NMR data are observed for residues Ile7, Leu8, Asn9, and Glu34. Residues 28 to 34 are not observed in the solid-state NMR spectra. These residues are located in the interface of the N-terminal dimerization domain and suggest small distortions of the dimer packing, which may be of functional significance, given its hinge character in the oligomer structure. The published structure of the 1-83 oligomer (PDB 3NR7) was analyzed using HingeProt to predict the residues defining hinges [32]. Focussing on pairs of molecules connected by the N-terminal dimerization domain, the two lowest frequency/high amplitude motional modes are predicted with residues 28 and 31 and 47-48 respectively as hinges (Fig. 7B). The first hinge is consistent with the region showing the largest chemical shift differences between solid-state and solution spectra. The second one agrees with the previous experimental data showing that the 1-47 construct forms the minimal dimerization domain. Not surprisingly, even small changes in the dimerization domain result in substantial displacement of the helix ends, where the second dimerization domain is located and the DNA binding domain is anchored. Thus, small conformational changes in the dimerization domain may change the exact oligomer structure and its capacity to recognize specific DNA geometries.

An example of structural differences between H-NS N-terminal dimers can be obtained by comparing the structures of the N-terminal domains of H-NS from *E. coli* and *V. cholera* [19]. The major difference between the two domains is that Asn9 is replaced by a leucine residue in *Vibrio cholerae* H-NS. Asn9 is one of the residues showing large chemical shift differences between solution and solid-state spectra of the *E. coli* H-NS N-terminal domain. Interestingly, the relative orientation of the H3 helices within the dimer is significantly different. The residues 24 and 45 that are separated by six complete helical turns

can be used to monitor the relative positions of the helices in the dimer. The distances between C α from residues Ser45 (Ala45 in *V. cholerae* H-NS) in the two symmetry related helices are, respectively, 37.7 Å and 38.2 Å in *E. coli* and *V. cholerae* H-NS. Conversely, the distances between Glu24 and its symmetry related counterparts are 27.4 Å and 25.9 Å the in *E. coli* and *V. cholerae* proteins. The changes in the distance spanned by residues situated at the end of the two helices H3 due to small changes in the N-terminal dimer interface will be further amplified in the complete protein. This distance will directly affect the separation of consecutive DNA binding regions along the H-NS oligomer. In the structure of the 1-83 oligomers, the distance between C α from equivalent Ser45 residues is 36.1 Å and increases to 91.5 between the Ala67 residues of the two molecules in the dimer. Assuming a direct proportionality, the distortions in the H3 helix between the *E. coli* and *V. cholerae* H-NS would represent a shift in the relative position of the DNA binding domain of around 4 Å. This may seem a modest number (just over the distance of one DNA base pair), but in a 8-mer (4-dimer) H-NS oligomer, the DNA domains of the end-terminal H-NS molecules would change by 16Å, which corresponds to around half the helical repeat of a DNA helix. Thus, a modest change in the relative orientation of the long H3 helices at the N-terminal dimerization site may result in the recognition of significantly different DNA structural features. We had previously shown that the complementary mutations Asn9Leu and Leu9Asn in full length *E. coli* and *V. cholerae* substantially change the electrophoretic mobility of the nucleoprotein complexes, confirming that even small changes in the N-terminal dimerization domain have a large effect in DNA binding [33]. Furthermore, Asn9 and Arg12 are involved in binding of Hha, a protein that modifies the capacity of H-NS to recognize horizontally acquired DNA [2].

Taken together, the existing evidence and the ssNMR data suggest that the N-terminal dimerization domain may act as functionally important hinge contributing to the capacity of

H-NS to recognize certain DNA classes, especially in the presence of co-regulators of the Hha family. ssNMR data gives the first structural information on the functionally important linker region that was absent in the truncated constructs studied previously. Our results further show that solid-state NMR provides a valuable tool to study H-NS oligomers and their interaction with co-regulators as well as its cognate DNA sequences.

Experimental procedures

Sample preparation and characterization. The (U- ^{13}C , ^{15}N)-labeled full length H-NS and H-NS 1-47 proteins from *E. coli* were obtained and purified as described elsewhere [7,33,34]. Saturated ammonium sulphate was slowly added to 70% saturation to 70-80 μM H-NS samples while gently stirring at 4°C. The precipitate was allowed to form for 1 h at 4°C. The sample was centrifuged at 4°C for 30 min at 4000 g and the supernatant was removed. Freshly prepared HNS precipitate samples were transferred into 3.2-mm MAS rotors by low-speed centrifugation packed with bottom and top spacers and subsequently analyzed by ssNMR spectroscopy. The microcrystalline samples were checked for native activity after redissolving them. *In vitro* oligomer formation was checked by size exclusion chromatography. The chromatograms were indistinguishable from those of the purified samples before precipitation, suggesting that the fresh and redissolved samples had similar oligomer distributions. Two binding events were checked in the recovered samples: DNA binding was measured by electrophoretic band-shift assays and Hha binding to the N-terminal domain was checked by the disappearance of NMR signals from Hha, as demonstrated previously [33,34] (Supplementary Information, Fig. S4). Electrophoretic band-shift assays were performed as described previously [33]. The 2.8 kbp DNA fragment

used, corresponding to the regulatory region of the *hly* operon of *E. coli*, was obtained by PCR amplification from plasmid pHly152 [33].

NMR spectroscopy. All ssNMR experiments were performed on a Bruker Avance standard bore 700 MHz instrument (Bruker Biospin, Germany), equipped with a 3.2 mm triple resonance (^1H , ^{13}C , ^{15}N) CP-MAS probehead. Two- and three-dimensional ^{13}C - ^{13}C and ^{15}N - ^{13}C correlation experiments were performed on uniformly ^{13}C , ^{15}N -labeled H-NS samples at different MAS frequencies. The probehead temperature was adjusted to ensure a constant sample temperature at around 4 °C. Heteronuclear polarization transfer was implemented using ramped Hartmann-Hahn cross-polarization (HHCP) either to generate the initial polarization (^1H - ^{13}C or ^1H - ^{15}N) or as a polarization step in the heteronuclear correlation experiment (^{15}N - ^{13}C) employing simultaneously continuous-wave (CW) decoupling on ^1H channel. The homonuclear two-dimensional ^{13}C - ^{13}C correlation experiments were performed using proton-driven spin diffusion under weak coupling conditions [25] (PDSD-WC) at a MAS frequency close to the rotational resonance condition for $\text{C}\alpha$ and C' resonances, *i.e.* 10.92 kHz at 16.4 T. Under this condition, spin-diffusion mixing times of 20 ms to 150 ms were typically used to reveal intraresidue and sequential correlations, respectively. For heteronuclear triple resonance experiments, ^{15}N - ^{13}C transfers were achieved by using SPECIFIC-CP [26, 34] steps of 3 ms, with a low radio-frequency field amplitude on the ^{13}C channel and a carrier frequency setted in the desired spectral region *i.e.* at 55 ppm for the NCACX experiment and 175 ppm to achieve selective polarization transfer from the nitrogen to the carbonyl region in the NCOCX experiment, followed by a ^{13}C - ^{13}C recoupling scheme. For the (U - ^{13}C , ^{15}N)-labeled H-NS (1-47) sample, the 2D NCACX experiment was performed at a MAS frequency of 17 kHz using PARIS [27] recoupling with proton rf recoupling of 5.5 kHz and a mixing time of 100 ms while the 2D NCOCX correlation spectrum was recorded

using MIRROR [28] recoupling with a proton rf recoupling and mixing times of 21 kHz /75 ms and 4 kHz/75 ms at a MAS frequency of 17 kHz. For the (U- ^{13}C , ^{15}N)-labeled full-length H-NS sample, the 2D ^{13}C - ^{13}C and ^{15}N - ^{13}C correlation spectra were recorded using 4 ms evolution times in indirect ^{13}C and ^{15}N dimensions, with 1024 to 1240 data points in the direct dimension, and 340 or 28 data points in the indirect dimension for PDS and NCACX spectra, respectively. Proton decoupling during all evolution and detection periods was implemented using SPINAL-64 scheme [36] at a power level of 83.3 kHz. All experiments were acquired by using a TPPI scheme in indirect dimension [37]. Data were Fourier transformed using a cosine-square window function with zero filling to 2048 data points in direct dimension and 2048 or 1024 data point in the indirect dimension for PDS and NCACX spectra, respectively. The 3D ^{15}N - ^{13}C - ^{13}C NCOCX experiment was recorded using 3.4 ms evolution time in indirect ^{15}N and ^{13}C dimensions and with 24 t_1 and t_2 increments and 992 scans, resulting in a total measuring time of 13.5 days. 3D NCOCX spectrum was Fourier transformed using cosine-square window function with zero filling to 2k data points in t_3 and 128 data points in t_1 and t_2 . All data were processed using TOPSPIN 3.0 software package (Bruker BioSpin) and analyzed with SPARKY [38]. ^{13}C and ^1H resonances were calibrated using adamantane as an external reference. The upfield ^{13}C resonance and isotropic ^1H resonance of adamantane were set to 31.47 and 1.7 ppm, respectively, to allow for a direct comparison of the solid-state chemical shifts to solution-state NMR data. Accordingly, ^{15}N resonances were calibrated using the tripeptide AGG [29] as an external reference.

Experimental chemical shifts of the H-NS 2-58 fragments were obtained from the BioMagResBank (BMRB 5390, PDB 1LR1). Although H-NS 1-47 solution NMR spectra had been assigned before the chemical shift values were not available and we remeasured them in a doubly labeled construct at 298K in 20 mM sodium phosphate (pH 7.0), 150 mM NaCl, 1 mM tris(2-carboxyethyl)-phosphine (TCEP), 0.2 mM ethylene diamine tetraacetic

acid (EDTA), 0.01 % (w/v) NaN₃ on a Bruker Avance 800 MHz instrument equipped with a TCI cryo-probe. Chemical shift assignments were obtained using a combination of ¹H-¹⁵N-HSQC, ¹H-¹³C-HSQC, CBCA(CO)NH and HCCH-TOCSY experiments and were referenced with respect to 4,4-dimethyl-4-silapentane-1-sulfonic acid (DSS). Structure analysis and figures were prepared using PYMOL [39].

Elastic Network models. We analyzed the X-ray structure of the H-NS 1-83 dimer using HingeProt [32] to predict hinges that coordinate low frequency collective modes on the basis of an elastic network model. Hinges often mediate functionally important motions in proteins [40]. Coarse-grained models along the first two dominant modes were reproduced with the use of *elNémo* [41].

Acknowledgments. The research leading to these results has received funding from the European Community's Seventh Framework Programme ([FP7/2007-2013] under grant agreements 211800 and 261863 and the Spanish Ministry of Science and Innovation-FEDER (BIO2010–15683). In addition, this work was funded in part by NWO (grants 700.26.121 and 700.58.102 to MB) and the Generalitat de Catalunya (2009SGR1352).

References

- 1 Wang W, Li GW, Chen C, Xie XS & Zhuang X (2011) Chromosome organization by a nucleoid-associated protein in live bacteria. *Science* **333**, 1445-1449.
- 2 Baños RC, Vivero A, Aznar S, Garcia J, Pons M, Madrid C & Juárez A (2009) Differential regulation of horizontally acquired and core genome genes by the bacterial modulator H-NS. *PLoS Genet.* **5**, e1000513.
- 3 Dorman CJ (2009) Horizontally acquired homologues of the nucleoid-associated protein H-NS: implications for gene regulation. *Mol Microbiol* **75**, 264-267.
- 4 Lucchini S, Rowley G, Goldberg MD, Hurd D, Harrison M & Hinton JC (2006) H-NS mediates the silencing of laterally acquired genes in bacteria. *PLoS Pathog* **2**, e81.
- 5 Bouffartigues E, Buckle M, Badaut C, Travers A & Rimsky S (2007). H-NS cooperative binding to high-affinity sites in a regulatory element results in transcriptional silencing. *Nat Struct Mol Biol* **14**, 441-448.

- 6 Dorman CJ (2004) H-NS: a universal regulator for a dynamic genome. *Nat Rev Microbiol* **2**, 391-400.
- 7 Cordeiro TN, Schmidt H, Madrid C, Juarez A, Bernado P, Griesinger C, Garcia J & Pons M (2011) Indirect DNA readout by an H-NS related protein: structure of the DNA complex of the C-terminal domain of Ler. *PLoS Pathog* **7**, e1002380.
8. Dame RT, Noom MC & Wuite GJ (2006) Bacterial chromatin organization by H-NS protein unravelled using dual DNA manipulation. *Nature* **444**, 387-390.
- 9 Liu Y, Chen H, Kenney LJ & Yan J (2010) A divalent switch drives H-NS/DNA-binding conformations between stiffening and bridging modes. *Genes Dev* **24**, 339-344.
- 10 Smyth CP, Lundback T, Renzoni D, Siligardi G, Beavil R, Layton M, Sidebotham J M, Hinton JC, Driscoll PC, Higgins CF & Ladbury JE (2000) Oligomerization of the chromatin-structuring protein H-NS. *Mol Microbiol* **36**, 962-972.
- 11 Castang S & Dove SL (2010) High-order oligomerization is required for the function of the H-NS family member MvaT in *Pseudomonas aeruginosa*. *Mol Microbiol* **78**, 916-931.
- 12 Gordon BR, Li Y, Wang L, Sintsova A, van Bakel H, Tian S, Navarre WW, Xia B & Liu J (2010) Lsr2 is a nucleoid-associated protein that targets AT-rich sequences and virulence genes in *Mycobacterium tuberculosis*. *Proc Natl Acad Sci USA* **107**, 5154-5159.
- 13 Esposito D, Petrovic A, Harris R, Ono S, Eccleston JF, Mbabaali A, Haq I, Higgins CF, Hinton JC, Driscoll PC & Ladbury JE (2002) H-NS oligomerization domain structure reveals the mechanism for high order self-association of the intact protein. *J Mol Biol* **324**, 841-850.
- 14 Renzoni D, Esposito D, Pfuhl M, Hinton JC, Higgins CF, Driscoll PC & Ladbury JE (2001) Structural characterization of the N-terminal oligomerization domain of the bacterial chromatin-structuring protein, H-NS. *J Mol Biol* **306**, 1127-1137.
- 15 Arold ST, Leonard PG, Parkinson GN & Ladbury JE (2010) H-NS forms a superhelical protein scaffold for DNA condensation. *Proc Natl Acad Sci USA* **107**, 15728-15732.
- 16 Gordon BR, Li Y, Cote A, Weirauch MT, Ding P, Hughes TR, Navarre WW, Xia B & Liu J (2011). Structural basis for recognition of AT-rich DNA by unrelated xenogeneic silencing proteins. *Proc Natl Acad Sci USA* **108**, 10690-10695.
- 17 Bloch V, Yang Y, Margeat E, Chavanieu A, Auge MT, Robert B, Arold S, Rimsky, S & Kochoyan M (2003) The H-NS dimerization domain defines a new fold contributing to DNA recognition. *Nat Struct Mol Biol* **10**, 212-218.
- 18 Shindo H, Iwaki T, Ieda R, Kurumizaka H, Ueguchi C, Mizuno T, Morikawa S, Nakamura H & Kuboniwa H (1995) Solution structure of the DNA binding domain of a nucleoid-associated protein, H-NS, from *Escherichia coli*. *FEBS Lett* **360**, 125-131.
- 19 Cerdan R, Bloch V, Yang Y, Bertin P, Dumas C, Rimsky S, Kochoyan M & Arold ST (2003) Crystal structure of the N-terminal dimerisation domain of VicH, the H-NS-like protein of *Vibrio cholerae*. *J Mol Biol* **334**, 179-185.
- 20 Andrew ER, Bradbury A & Eades RG (1958) Nuclear magnetic resonance spectra from a crystal rotated at high speed. *Nature* **182**, 1659.
- 21 Lipton AS, Buchko GW, Sears JA, Kennedy MA & Ellis PD (2001) Zn⁶⁷ solid-state NMR spectroscopy of the minimal DNA binding domain of human nucleotide excision repair protein XPA. *J Am Chem Soc* **123**, 992-993.
- 22 Lorieu JL, Day LA & McDermott AE (2008) Conformational dynamics of an intact virus: order parameters for the coat protein of Pf1 bacteriophage. *Proc Natl Acad Sci USA* **105**, 10366-10371.

- 23 Böckmann A, Lange A, Galinier A, Luca S, Giraud N, Heise H, Juy M, Montserret R, Penin F & Baldus M (2003) Solid-state NMR sequential resonance assignments and conformational analysis of the 2*10.4 kDa dimeric form of the *Bacillus subtilis* protein Crh. *J Biomol NMR* **27**, 323-339.
- 24 Pauli J, Baldus M, van Rossum B, de Groot H & Oschkinat H (2001) Backbone and side-chain C¹³ and N¹⁵ signal assignments of the alpha-spectrin SH3 domain by magic angle spinning solid-state NMR at 17.6 tesla. *ChemBioChem* **2**, 272-281.
- 25 Seidel K, Lange A, Becker S, Hughes CE, Heise H & Baldus M (2004) Protein solid-state NMR resonance assignments from (¹³C,¹³C) correlation spectroscopy. *Phys Chem Chem Phys* **6**, 5090-5093.
- 26 Baldus M, Petkova AT, Herzfeld J & Griffin RG (1998) Cross polarization in the tilted frame: assignment and spectral simplification in heteronuclear spin systems. *Mol Physics* **95**, 1197-1207.
- 27 Weingarh M, Demco DE, Bodenhausen G & Tekely P (2009) Improved magnetization transfer in solid-state NMR with fast magic angle spinning. *Chem Phys Lett* **469**, 342-348.
- 28 Scholz I, Huber M, Manokilas T, Meier BH & Ernst M (2008). MIRROR recoupling and its application to spin diffusion under fast magic-angle spinning. *Chem Phys Lett* **460**, 278-283.
- 29 Luca S, Filippov DV, van Boom JH, Oschkinat H, de Groot HJM & Baldus M (2001) Secondary chemical shifts in immobilized peptides and proteins: A qualitative basis for structure refinement under magic angle spinning. *J Biomol NMR* **20**, 325-331.
- 30 Shindo H, Ohnuki A, Ginba H, Katoh E, Ueguchi C, Mizuno T & Yamazaki T (1999) Identification of the DNA binding surface of H-NS protein from *Escherichia coli* by heteronuclear NMR spectroscopy. *FEBS Lett* **455**, 63-69.
- 31 Fernández-de-Alba C, Berrow NS, Garcia-Castellanos R, García J, & Pons M (2013) On the origin of the selectivity of plasmidic H-NS towards horizontally acquired DNA: linking H-NS oligomerization and cooperative DNA binding. *J. Mol. Biol.* 10.1016/j.jmb.2013.03.006.
- 32 Emekli U, Schneidman-Duhovny D, Wolfson HJ, Nussinov R & Haliloglu T. (2008) HingeProt: Automated Prediction of Hinges in Protein Structures. *Proteins*, **70**,1219-1227.
- 33 Garcia J, Madrid C, Cendra M, Juarez A & Pons M (2009) N9L and L9N mutations toggle Hha binding and hemolysin regulation by *Escherichia coli* and *Vibrio cholerae* H-NS. *FEBS Lett* **583**, 2911-2916.
- 34 Garcia, J, Madrid C, Juarez A & Pons M (2006) New roles for key residues in helices H1 and H2 of the *Escherichia coli* H-NS N-terminal domain: H-NS dimer stabilization and Hha binding. *J Mol Biol* **359**, 679-689.
- 35 Petkova AT, Baldus M, Belenky M, Hong M, Griffin RG & Herzfeld J (2003) Backbone and side chain assignment strategies for multiply labeled membrane peptides and proteins in the solid state. *J Magn Reson* **160**, 1-12.
- 36 Fung BM, Khitritin AK & Ermolaev K (2000) An improved broadband decoupling sequence for liquid crystals and solids. *J Magn Reson* **142**, 97-101.
- 37 Marion D & Wuthrich K (1983) Application of phase sensitive two-dimensional correlated spectroscopy (COSY) for measurements of H¹-H¹ spin-spin coupling-constants in proteins. *Biochem Biophys Res Comm.***113**, 967-974.
- 38 Goddard TD & Kneller DG. SPARKY 3. University of California, San Francisco.
- 39 DeLano WL (2002) The PyMOL Molecular Graphics System.
- 40 Bahar I (2010) On the functional significance of soft modes predicted by coarse-grained models for membrane proteins *J Gen Physiol* **135**, 563-573

- 41 Suhre K & Sanejouand Y-H (2004) ElNemo: a normal mode web server for protein movement analysis and the generation of templates for molecular replacement. *Nucleic Acids Research*, **32**, 610-614

Supporting Information.

The following supplementary material is available:

Table S1. Solid-state NMR chemical shifts of self-assembled (U-¹³C,¹⁵N)-labeled full-length H-NS.

Table S2. Solid-state NMR chemical shifts of (U-¹³C,¹⁵N) H-NS 1-47.

Table S3. ¹H, ¹³C and ¹⁵N solution NMR chemical shifts of (U-¹³C,¹⁵N) H-NS 1-47.

Fig. S1. 2D NCOCX correlation spectrum obtained on (U-¹³C,¹⁵N) full-length H-NS.

Fig. S2. Overlay of the 2D ¹³C-¹³C correlation spectra obtained on (U-¹³C,¹⁵N)-labeled full-length H-NS and its truncated variant H-NS 1-47.

Fig. S3. Histogram representation of C α secondary chemical shifts and chemical shift differences between H-NS 1-47 in solid state and in solution and solid state H-NS 1-137.

Fig. S4. Functional assays on full length H-NS samples.

Figure legends

Fig. 1: Two-dimensional ssNMR correlation spectra of self-assembled (U-¹³C,¹⁵N)-labeled H-NS oligomers (A) Aliphatic region of the proton-driven ¹³C-¹³C spin diffusion (PDS) spectrum recorded with 20 ms mixing time. (B) NCACX correlation spectrum recorded using a SPECIFIC-CP of 4 ms for the ¹⁵N - ¹³C α transfer step and a PDS mixing of 20 ms to transfer the magnetization from ¹³C α to side-chain ¹³C resonances. Assigned residues as well as regions of significant overlap for certain residue types are indicated in black and red, respectively. All spectra were recorded at 700 MHz proton Larmor frequency, 10.92 kHz MAS frequency and at a sample temperature of 275 K.

Fig. 2: ssNMR characterization of the H-NS dimerization domain H-NS 1-47 (A) Overlay of the 2D ¹³C-¹³C PDS correlation spectra obtained on (U-¹³C,¹⁵N)-labeled full-length H-NS (black) and its truncated variant H-NS 1-47 (green) using a PDS mixing time of 20 ms (10.92 kHz MAS, 700 MHz, 275 K). Labels indicate characteristic intra-residue CC correlations of Thr (I to IX) and Pro (X to XII) residues from the N-terminal domain H-NS 2-47 (green) and other topological regions (black). (B) Distribution of Thr, Pro and Ser residues throughout the protein sequence using the same color code as in (A) and showing secondary structure elements (α -helix as cylinders and β -sheet as arrow) as found in available 3D structures of isolated H-NS domains. Protein regions for which no structural information is available are indicated as dashed lines.

Fig. 3. Exemple of sequential assignment of the protein segment C21-L26 based on two-dimensional homonuclear and heteronuclear ssNMR spectroscopy on (U-¹⁵N,¹³C)-labeled H-NS 1-47 preparation. (A) 2D (¹³C-¹³C) correlation spectra obtained under weak

coupling conditions using PDSM mixing times of 20 ms (black) and 150 ms (red) at a MAS frequency of 10.92 kHz and 700 MHz ^1H Larmor frequency. (B) 2D (^{15}N , ^{13}C) NCACX and (C) 2D (^{15}N , ^{13}C) NCOCX correlation spectra recorded at a MAS frequency of 17 kHz using respectively PARIS and MIRROR recoupling of 100 and 150 ms. Assignments are indicated in rectangles. Characteristic sequential (i , $i\pm 1$) and (i , $i\pm 2$) correlations are highlighted in red and green, respectively. Dashed lines indicate CC and NC connectivities.

Fig. 4. Sequential assignment of ($\text{U-}^{15}\text{N}$, ^{13}C)-labeled full-length H-NS (A) Strip plot from 3D NCOCX spectrum recorded on ($\text{U-}^{13}\text{C}$, ^{15}N)-labeled full-length H-NS showing $^{15}\text{N}(i)$ - $^{13}\text{C}_{\text{aliph}}(i-1)$ correlations for residues in the N-terminus domain of H-NS. (B) Overlay of the 2D (^{13}C , ^{13}C) PDSM correlation spectra obtained on ($\text{U-}^{13}\text{C}$, ^{15}N)-labeled full length H-NS using 20 ms (black) and 150 ms (red) PDSM mixing times under weak coupling conditions (700 MHz, 10.92 kHz MAS, 275 K). Assignments are indicated in rectangles. Characteristic sequential (i , $i\pm 1$) and (i , $i\pm 2$) correlations are highlighted in red and green, respectively. Solid lines indicate sample sequential walk from residue 68 to 74 using only intraresidue and sequential CC correlations.

Fig. 5. Secondary structure analysis of H-NS oligomers (A) Secondary chemical shifts ($\Delta\delta\text{C}\alpha$ - $\Delta\delta\text{C}\beta$) of H-NS with reference to average values taken from Biological Magnetic Resonance Data Bank (BMRB; <http://www.bmrb.wisc.edu>). Positive values indicate helical structure (H) whereas negative values indicate β -sheet-like (S) or unstructured protein regions. (B) Secondary structure elements within self-assembled full-length H-NS as revealed by ssNMR (red) are given as horizontal bars below, using H and S for α -helical and β -sheet

protein segments, respectively and are compared to those seen in available 3D models of isolated H-NS domains (grey).

Fig. 6. Analysis of the intraresidue threonine correlation pattern. (A) *Left*, Spectral region extracted from the 2D ^{13}C - ^{13}C PDS correlation spectrum showing $\text{C}\alpha$ - $\text{C}\beta$ cross-peaks of H-NS threonines. Assignment is given when available. Unassigned cross-peaks are labeled with roman numbers. *Middle*, histogram representation of C' , $\text{C}\alpha$ and $\text{C}\beta$ secondary chemical shifts of threonines. Secondary chemical shifts ($\Delta\delta^{13}\text{C}$) were calculated using averaged chemical shifts ($\delta^{13}\text{C}_{\text{AVE}}$) from the BioMagResBank and experimental ssNMR chemical shifts ($\delta^{13}\text{C}_{\text{EXP}}$) using the $\Delta\delta^{13}\text{C} = \delta^{13}\text{C}_{\text{EXP}} - \delta^{13}\text{C}_{\text{AVE}}$ [29]. *Right*, relative intensity of Thr $\text{C}\alpha$ - $\text{C}\beta$ cross-peaks (B) Position of threonine residues throughout H-NS protein sequence and secondary structure elements. (C) Topological organization of H-NS and associated biological functions. Color code: red, α -helical segments; green, β -sheet segments.

Fig. 7. H-NS dimer hinge role suggested by comparison of solid-state NMR data with solution NMR data from the isolated dimerization domains of *E. coli*. (A) Solid-state NMR $\text{C}\alpha$ chemical shifts of full length H-NS compared with solution chemical shifts measured in H-NS 1-47. Residues with an agreement of $\Delta\delta\text{C}\alpha$ within ± 2 ppm are shown in green. Deviations greater than 2 ppm are highlighted in red and unassigned residues are indicated in grey. (B). Hinge motion predicted from the structure of H-NS 1-83 dimers using HingeProt. Top: hinge motion around residues 28 and 31*. Bottom: hinge motion around residues 47 and 48*. Asterisks refer to residues from the second chain in the dimer.